

Detection of Oscillations in a Type-I X-Ray Burst of 4U 0614+091 with SVOM/ECLAIRs

SÉBASTIEN LE STUM ,¹ FLORIANE CANGEMI,¹ ALEXIS COLEIRO,¹ SÉBASTIEN GUILLOT,² JÉRÔME CHENEVEZ,³

PHILIPPE BACON,¹ NICOLAS BELLEMONT,¹ LAURENT BOUCHET,² TRISTAN BOUCHET,⁴ CÉCILE CAVET,¹
 BERTRAND CORDIER,⁵ ANTOINE FOISSEAU,¹ OLIVIER GODET,² ANDREA GOLDWURM,^{6,7} XUHUI HAN,⁸ CYRIL LACHAUD,¹
 ZHAOSHENG LI,⁹ HUALI LI,⁸ YULEI QIU,⁸ JÉRÔME RODRIGUEZ,⁵ WENJUN TAN,¹⁰ LIAN TAO,¹⁰ LAURYNE VERWAERDE,¹
 CHENWEI WANG,¹⁰ JING WANG,⁸ JIANYAN WEI,⁸ CHAO WU,⁸ WENJIN XIE,⁸ LIPING XIN,⁸ SHAOLIN XIONG,¹⁰
 SHUANGNAN ZHANG,¹⁰ SHIJIE ZHENG,¹⁰

¹ Université Paris Cité, CNRS, Astroparticule et Cosmologie, F-75013 Paris, France

² IRAP, Université de Toulouse, CNRS, CNES, 9 avenue du Colonel Roche, BP 44346, F-31028 Toulouse Cedex 4, France

³ DTU Space, Technical University of Denmark, Elektrovej 327-328, DK-2800 Kongens Lyngby, Denmark

⁴ Université Paris Cité, Université Paris-Saclay, CEA, CNRS, AIM, 91191 Gif-sur-Yvette, France

⁵ Université Paris-Saclay, Université Paris Cité, CEA, CNRS, AIM, 91191 Gif-sur-Yvette, France

⁶ Université Paris Cité, CNRS, CEA, Astroparticule et Cosmologie, F-75013 Paris, France

⁷ CEA Paris-Saclay, Irfu/Département d'Astrophysique, 91191 Gif-sur-Yvette, France

⁸ National Astronomical Observatories, Chinese Academy of Sciences, Beijing 100101, China

⁹ Key Laboratory of Stars and Interstellar Medium, Xiangtan University, Xiangtan 411105, Hunan, China

¹⁰ Institute of High Energy Physics, Chinese Academy of Sciences, 19B Yuquan Road, Beijing 100049, China

Submitted to APJL

ABSTRACT

On 2025 January 10, a thermonuclear (Type I) X-ray burst from the neutron star low-mass X-ray binary *4U 0614+091* was detected with the ECLAIRs instrument on board the *SVOM* mission. We present here a time-resolved spectroscopic analysis of the burst, along with the detection of burst oscillations within a 51-second interval during the decay phase. The oscillation frequency is measured to be $\nu = 413.674 \pm 0.002$ Hz, consistent with previous reports. However, we detect a significant downward frequency drift over the burst duration, characterized by $\dot{\nu} = (-4.7 \pm 0.3) \times 10^{-3}$ Hz s⁻¹. This frequency evolution is atypical compared to those observed in similar burst oscillation sources. We tentatively attribute the observed drift to a Doppler shift induced by orbital motion. Under this interpretation, the inferred orbital period must be shorter than 20 minutes, placing *4U 0614+091* among the most compact known low-mass X-ray binaries.

Keywords: X-ray bursts, Compact binary stars, Low-mass x-ray binary stars

1. INTRODUCTION

Low-mass X-ray binaries (LMXBs) hosting neutron star accretors are known to exhibit intense, short-duration outbursts resulting from thermonuclear fusion of accreted material on the neutron star surface. These bursts typically present lightcurves characterized by a rapid rise in flux followed by a cooling tail lasting tens

of seconds (Galloway et al. 2020). In some cases, thermonuclear bursts exhibit coherent oscillations, referred to as burst oscillations (Strohmayer et al. 1996). In systems where a persistent pulsation is also observed, burst oscillation frequencies are found to be close to the spin frequency of the neutron star, indicating a strong connection between the two phenomena (see Watts 2012, for a review).

The LMXB 4U 0614+091 is an ultracompact system composed of a neutron star and a white dwarf companion. The distance to it has been estimated to be

$3.3^{+1.3}_{-2.4}$ kpc based on the GAIA parallax of its optical counterpart (Arnason et al. 2021); or 2.59 ± 0.03 kpc under the hypothesis that a photospheric radius expansion burst detected in 2001 was emitting at the Eddington luminosity with a pure He composition (Galloway et al. 2020). In the following, an approximate distance of 3 kpc is chosen for the relevant computations. Evidence of quasi-periodic oscillations (QPO, Ford et al. 1997) and of an accretion-powered compact radio jet (Migliari et al. 2010) have been observed. Constraints on the neutron star mass, derived from the maximum observed QPO frequency, suggest a mass of approximately $2 M_{\odot}$ (Boutelier et al. 2009; van Doesburgh et al. 2018). Spectroscopic studies indicate that the accretion flow from the white dwarf is rich in carbon and oxygen but deficient in hydrogen and helium (Nelemans et al. 2004; Madej et al. 2014). However, the observed burst recurrence rate implies that a non-negligible fraction of helium must be present in the accreted material (Kuulkers et al. 2010). Despite extensive study, the orbital period of 4U 0614+091 remains uncertain. Optical photometry has revealed a modulation with a period of approximately 50 minutes (Shahbaz et al. 2008), while Madej et al. (2013) report a periodicity of approximately 30 minutes in the 4650 Å oxygen line. Alternatively, Baglio et al. (2014) argue for an orbital period $\gtrsim 1$ hour, based on the assumption that the modulation arises from the outer rim of the accretion disk.

Burst oscillations at a frequency of 414.75 Hz were previously detected in 4U 0614+091 during an October 2006 burst observed with the Swift/BAT instrument (Strohmayer et al. 2008). Additionally, a possible oscillation signal near 413 Hz was reported from a burst detected by the GECAM instrument (Chen et al. 2022) in January 2021.

In this Letter, we present the detection of burst oscillations at a frequency of 413.674 ± 0.002 Hz using the ECLAIRs X-ray telescope on board the Space-based multi-band astronomical Variable Object Monitor (SVOM) satellite. Section 2 provides a brief overview of the instrument and the analysis methods. The results of the time-resolved spectroscopy and oscillation search are presented in Section 3, followed by a discussion of their interpretation in Section 4 and conclusions in Section 5.

2. DATA SET

SVOM is a Chinese-French space mission, launched on June 22nd, 2024, designed to explore the high-energy transient sky (Wei et al. 2016). The satellite is equipped with four instruments: the Microchannel X-Ray Telescope (MXT), a soft X-ray (0.2 to 10 keV) instrument using micro-pore optics (lobster eyes, Götz et al. 2014);

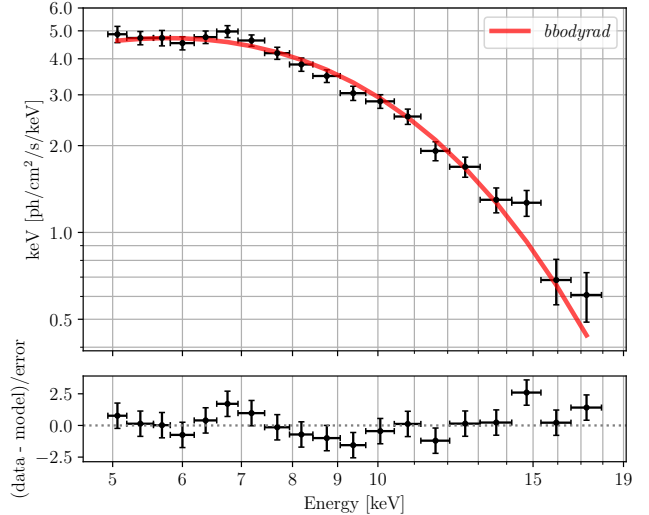


Figure 1. Time-integrated spectrum between $T = T_0$ and $T = T_0 + 25$ s, with in red a fitted *bbodyrad* model with $kT = 2.04$ keV.

the Gamma Ray Burst Monitor (GRM), a set of three detectors sensitive to photons in the 15 keV to 5 MeV range (Dong et al. 2010); the Visible Telescope (VT, Wu et al. 2012), a 40 cm optical telescope with two channels (blue and red); and ECLAIRs, a large field of view (FoV) of 89° by 89° coded-mask telescope (Goldwurm & Gros 2022) operating in the 4 to 150 keV range with a $10\ \mu\text{s}$ timing resolution (Godet et al. 2014). The satellite's primary objective is the detection and characterisation of Gamma-Ray Bursts. To this end, ECLAIRs operates an onboard triggering system that identifies fast transient events and determines their sky position. If the trigger corresponds to a source not listed in the onboard catalog, the system can autonomously request a rapid reorientation (slew) of the spacecraft to enable follow-up observations (Dagoneau et al. 2020; Dagoneau & Schanne 2022).

On 2025-01-10, the ECLAIRs onboard system detected a significant excess with a signal-to-noise ratio of 47 in an image integrated over a 20.48-second interval, starting at $T_0 = 2025-01-10T15:58:03$ UTC, in the 5–8 keV energy band. This detection triggered an alert with coordinates consistent with the known source 4U 0614+091, located 22.3° from the center of the FoV. As the source was listed in the onboard catalog, no satellite slew was initiated in response to the trigger. At the time of the trigger, the Earth was outside the telescope's FoV, and the spacecraft was approaching the South Atlantic Anomaly (SAA), resulting in an increasing background count rate due to charged particle flux.

2.1. Data analysis

The reduction and analysis of ECLAIRs data for 4U 0614+091 were performed using the ECLAIRs Pipeline (ECPI), developed for the mission science ground segment (Goldwurm et al., in preparation), which enables both imaging and spectroscopic analysis from event data. As a first step, good time intervals (GTIs) were selected based on satellite attitude stability and instrumental conditions. Around the relevant period for this work, the GTIs were uninterrupted. Calibrated detector-plane images were then generated in a set of energy bins between 4 and 30 keV. Detector images in a few large energy bins were spatially deconvolved using the coded-mask pattern to produce sky images. A point-source extraction algorithm was subsequently applied to the sky images to fit the positions of all sources within the FoV. Using the fitted position ensures the accurate modeling of sources for the spectral extraction and event selection, avoiding effects of biases in the telescope orientation with respect to the satellite's attitude. Sources count rates were derived in 30 smaller, logarithmically spaced, energy bins by modeling the contributions to each detector pixel from both 4U 0614+091 and the Crab Nebula, the only other bright source present in the FoV, and simultaneously fitting them to the binned detector images. A background component, modeled as a 2-D polynomial, was also included in the fit.

3. RESULTS

3.1. Spectroscopy

The source count rate spectrum, derived by the procedure described above, was fitted using XSPEC version 12.15.0 (Arnaud 1996), with a χ^2 minimization method. The uncertainties on spectral parameters were computed at the 90% confidence level. A time-integrated spectrum, covering the interval from T_0 to $T_0 + 25$ s, is shown in Figure 1, where the best-fit `bbodyrad` model is overlaid on the data. Applying a 2% systematic uncertainty, the fit yields a reduced chi-squared of $\chi_r^2 = 19.7/17 = 1.16$. The inclusion of an additional power-law component does not significantly improve the fit, meaning that we are unable to study the non-thermal contribution to the spectrum. Residuals in the spectrum show some features, but it is unclear whether these arise from still uncorrected instrumental systematics or from physical effects, such as absorption edges similar to those reported in GRS 1747–312 by Li et al. (2018). The best-fit parameters are a black-body temperature of $kT = 2.04 \pm 0.04$ keV and an apparent emission radius of $R = 5.8 \pm 0.3$ km, assuming a source distance of 3 kpc. From this model, we derive a time-integrated bolometric burst energy of

$E_{\text{bol}} = (1.89 \pm 0.04) \times 10^{39}$ erg, corresponding to a fluence of $F_{\text{bol}} = (1.75 \pm 0.04) \times 10^{-6}$ erg cm $^{-2}$. These values are consistent with typical bursts from this source, as reported in Table 2 of Kuulkers et al. (2010).

The source exhibits a significant accretion emission around the burst. Between 2025-01-10T13:46:13 (start of the observation) and 2025-01-10T15:57:52 ($T_0 - 11$ s), with an exposure of 2.7 ks, its spectrum is well described ($\chi_r^2 = 5.5/7 = 0.79$) by a power-law with a photon index of 2.65 ± 0.20 and a flux between 4 and 30 keV of $1.2_{-0.4}^{+0.1} \times 10^{-9}$ erg cm $^{-2}$ s $^{-1}$. After the burst, between 2025-10-01T16:48:34 and 2025-10-01T21:38:25 (end of the observation), with an exposure of 9.6 ks, its photon index is 2.97 ± 0.12 and its 4–30 keV flux is $1.41_{-0.19}^{+0.04} \times 10^{-9}$ erg cm $^{-2}$ s $^{-1}$ ($\chi_r^2 = 7.4/6 = 1.23$). On a longer timescale, between 2024 October 23 and 2025 March 3, the source was within the ECLAIRs FoV for a total of 117 ks of GTIs, excluding the observations previously mentioned. The time-integrated persistent emission spectrum is well described by a power-law with a photon index of 2.77 ± 0.12 , yielding a reduced chi-squared of $\chi_r^2 = 4.7/11 = 0.43$. The corresponding average persistent flux in the 4–30 keV range is $1.48_{-0.16}^{+0.07} \times 10^{-9}$ erg cm $^{-2}$ s $^{-1}$. No additional Type I bursts were detected by ECLAIRs during this period.

The results of a time-resolved spectral analysis during the burst are shown in Figure 2, which presents the evolution of the flux, blackbody temperature, and apparent emission radius, assuming a source distance of 3 kpc. The analysis was performed using 2-second time bins starting from T_0 . The 4–30 keV flux peaks at $1.70 \pm 0.04 \times 10^{-7}$ erg cm $^{-2}$ s $^{-1}$, which is two orders of magnitude higher than the persistent flux, and is equivalent to 7.1 times the Crab flux in this energy range. The associated peak bolometric luminosity is $(2.09 \pm 0.07) \times 10^{38}$ erg s $^{-1}$, still assuming a distance of 3 kpc. A clear cooling trend is observed between $T_0 + 3$ s and $T_0 + 15$ s, with the blackbody temperature decreasing from $kT = 2.43 \pm 0.08$ keV to $kT = 1.60 \pm 0.09$ keV. Beyond this point, the temperature appears to reach a plateau; however, due to the lower flux levels, it becomes difficult to identify any significant trend. No evidence of photospheric radius expansion was found, as the radius remains constant within error bars. After $T_0 + 25$ s, the source is too faint to allow for a reliable spectral modeling.

3.2. Burst Oscillations

Contrary to the spectral analysis, where the contribution of each source is obtained from the number of counts in each pixel, an oscillation search requires studying the arrival times of photons at an individual level.

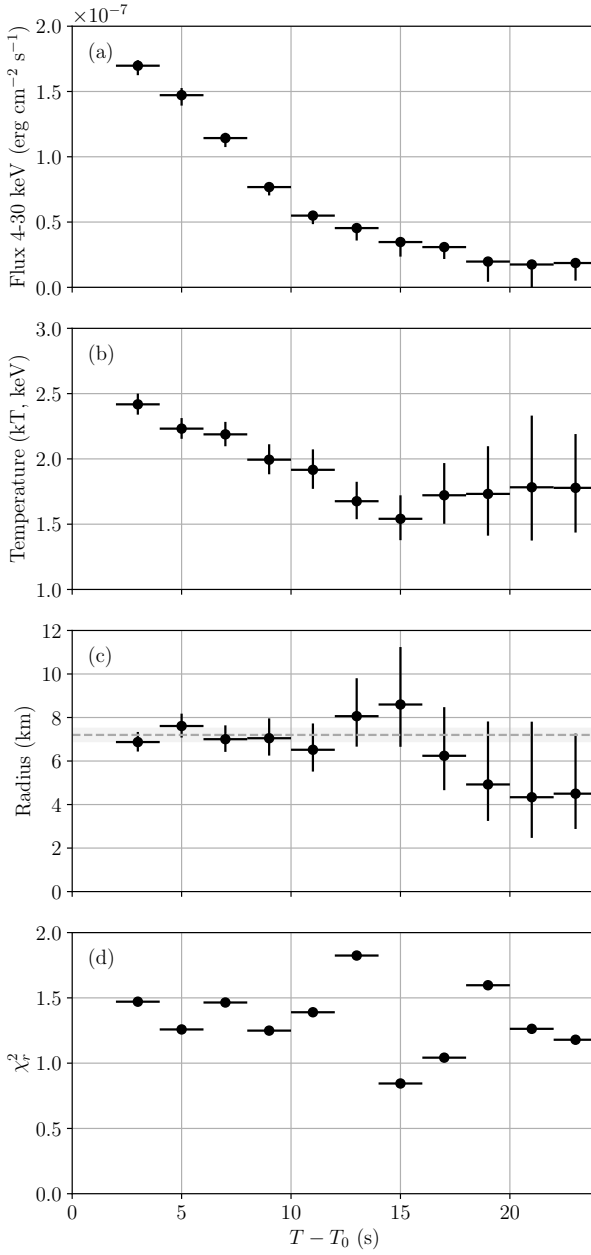


Figure 2. Evolution of time-resolved spectroscopy with a *bbodyrad* model, with (a) the flux between 4 and 30 keV, (b) the temperature kT , (c) the emission radius, assuming a distance of 3 kpc, with a constant radius shown as a dashed line, and (d) the reduced chi square $\chi^2_r = \chi^2/17$ degrees of freedom.

Thus, a selection of photons with respect to their position on the detector plane is performed to maximize the signal-to-noise ratio. Two primary sources of background noise in the timing analysis are (i) the elevated particle background due to the spacecraft's proximity to the SAA at the time of the burst, and (ii) the presence of the Crab Nebula within the ECLAIRs FoV. The coded-

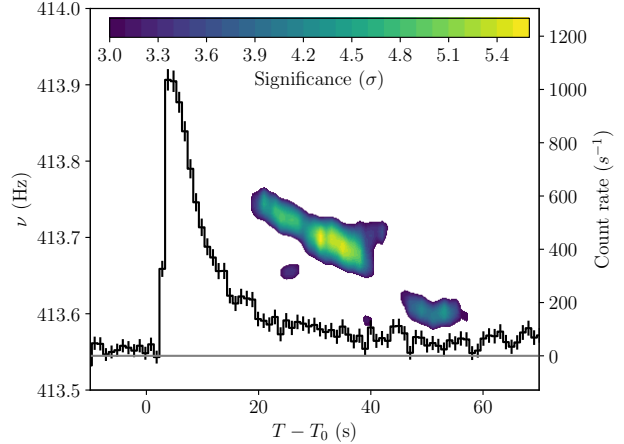


Figure 3. Significance contours of the oscillations as a function of time and frequency (left-hand axis), computed using a Z_1^2 test in a 20-second sliding window with 1-second steps. Significance levels are given as a color gradient. The burst light curve is shown as the equivalent on-axis count rate (right-hand axis) in the 4–40 keV energy band, with the persistent emission subtracted, binned in 1-second intervals.

mask pattern casts a shadow on the detector plane, such that each pixel has an illumination fraction, defined as 1 for full illumination by a source and 0 for full occultation by the mask. To obtain a clean sample of photons for the oscillation search, we selected events from detector pixels with an illumination fraction greater than 0.9 for 4U 0614+091 and less than 0.1 for the Crab. Additionally, events selected within the 4–40 keV energy range. The lower bound corresponds to the instrument's detection threshold, while the upper bound maximizes the signal-to-noise ratio, as the thermal spectrum of the burst is not expected to contribute significantly at higher energies.

Photon arrival times were corrected to the Solar System barycenter using the *light_travel_time* routine from the *astropy* library version 6.1.7 (Astropy Collaboration et al. 2022). The position of the satellite is recorded as a housekeeping data stream sampled every 1 second. The time correction difference between each sample is at most 3.4×10^{-5} s. This time resolution is sufficient to search for oscillations with periods much longer than this sampling interval, without requiring interpolation of the spacecraft's position. Additionally, the radial velocity of the satellite relative to the source remains nearly constant over the short burst interval (tens of seconds). As a result, any residual error in the barycentric correction would introduce only a small Doppler shift in the oscillation frequency, without significantly affecting the coherence or detectability of the signal.

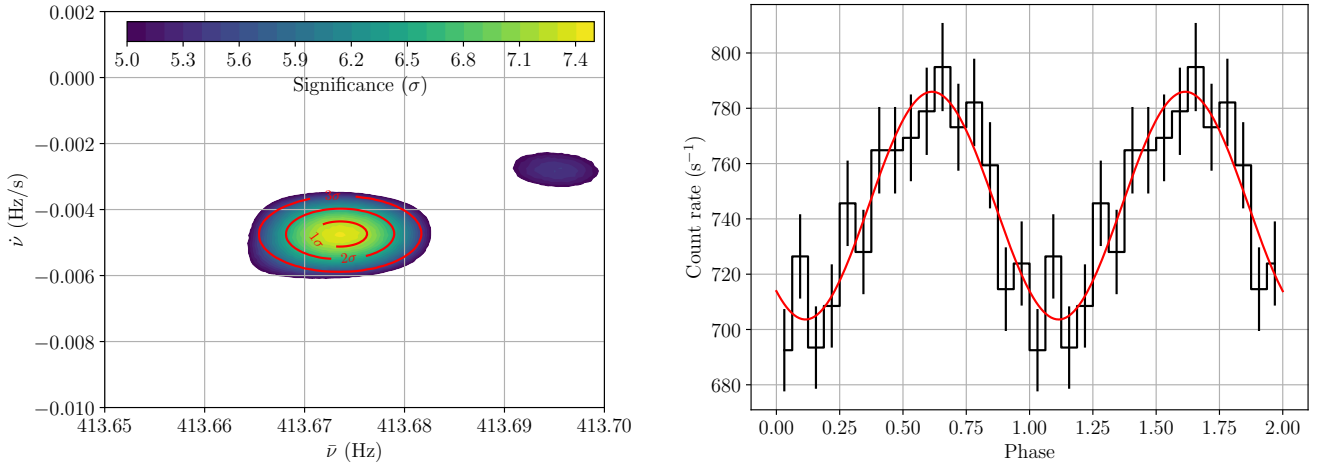


Figure 4. **Left:** Significance contours in the $\bar{\nu}$ – $\dot{\nu}$ plane for the time window yielding the most significant signal [T_0+11 s, T_0+62 s]. Significance levels are given as a color gradient. Overlaid in red are the contours of a two-dimensional Gaussian fitted around the peak. The best-fit parameters, $\bar{\nu} = 413.674$ Hz and $\dot{\nu} = -4.7 \times 10^{-3}$ Hz/s, are used to fold the light curve in this interval. **Right:** Folded burst profile using the fitted parameters over the selected time window, in black. The best-fit sinusoidal model to the profile is shown in red

The search for burst oscillations is performed using the Z_n^2 statistics (Buccheri et al. 1983) implemented in the *stingray* package, version 2.2.6 (Bachetti et al. 2024a). Under the null (background-only) hypothesis, the Z_n^2 test follows a χ^2 distribution with $2n$ degrees of freedom, where n is the number of harmonics considered in the test. From this assumption, the probability of obtaining a given Z_n^2 value under the null hypothesis can be computed. The final significance (p-value) is then obtained by accounting for the number of independent trials performed in the frequency search.

Following the previous findings from Swift/BAT (Strohmayer et al. 2008) and GECAM (Chen et al. 2022) of significant burst oscillations at 414.7 Hz and 413.63 Hz, respectively, we searched for oscillations between 413 and 415 Hz using a resolution of 0.01 Hz. Assuming that the oscillating signal may only be present during a portion of the burst, we searched for the time window and the frequency that maximize a Z_1^2 test between $T_0 - 5$ s and $T_0 + 70$ s in this frequency range. Time windows are defined by varying their start and end times in 1-second increments, yielding a total of 2925 distinct intervals. We find the most significant signal in the time window [$T_0 + 27$ s, $T_0 + 43$ s] with a frequency of $\nu = 413.69$ Hz. The corresponding pre-trial p-value is 4.86×10^{-9} (5.85σ). After accounting for the number of trials across both frequency and time dimensions, the post-trial p-value is 2.41×10^{-3} (3.03σ significance). We note that this post-trial significance is conservative, as it assumes all trials are statistically independent.

Figure 3 shows the significance contours of the detected oscillation, computed using a 20-second sliding time window and overlaid on the burst light curve with the persistent emission subtracted. The persistent level is estimated by extrapolating the pre-burst count rate, thus including contributions from both the background and any steady emission from 4U 0614+091. This subtraction is performed for visualization purposes and does not affect the timing analysis itself. Figure 3 shows a possible decrease in the oscillation frequency over time, which we examine and discuss in Section 3.3.

3.3. Oscillation Frequency Drift

To investigate the possibility of a frequency drift during the burst, we introduced the frequency derivative $\dot{\nu}$ as an additional parameter in the burst oscillation search. The phase of each photon with arrival time t_j is then defined as $\phi_j = 2\pi(\nu t_j + \dot{\nu}t_j^2/2)$, which is then used to compute the Z_1^2 statistic.¹ A validation of this analysis procedure using the Crab pulsar is described in Appendix A. We scanned $\dot{\nu}$ in the range from -0.01 Hz/s to $+0.01$ Hz/s in steps of 0.001 Hz/s. We find the most significant signal in the time window [$T_0 + 11$ s, $T_0 + 62$ s] with a frequency at $T = T_0 + 11$ s of $\nu_0 = 413.80$ Hz and $\dot{\nu} = -0.005$ Hz/s. This signal has a pre-trial p-value of 7.69×10^{-13} (7.16σ), corresponding to a post-trial p-value of 4.20×10^{-6} (4.6σ), demonstrating a clear improvement of significance compared

¹ The standard search described previously corresponds to the special case where $\dot{\nu} = 0$.

to the constant-frequency search. For comparison, the significance of the signal in this time window for $\dot{\nu}=0$ drops to 4.2σ (1.85σ) pre (post) trial. Similarly, the significance of the signal for $\dot{\nu} = -0.005$ Hz/s in the time window found in Section 3.2 is 5.33σ (3.00σ) pre (post) trial, which is consistent with previous results. This is expected, as a frequency drift becomes more distinguishable from a constant-frequency signal when the analyzed time window is sufficiently long.

Figure 4 (left panel) shows the significance of the signal with respect to its average frequency $\bar{\nu}$ and its frequency derivative $\dot{\nu}$, in $[T_0 + 11\text{ s}, T_0 + 62\text{ s}]$. The central feature, around the point of maximum significance, is well described by a two-dimensional Gaussian function from which we can estimate the uncertainties on both the average frequency and the frequency derivative. We obtain the average frequency in the $[T_0+11\text{ s}, T_0+62\text{ s}]$ time window $\bar{\nu} = 413.674 \pm 0.002$ Hz and a refined value of $\dot{\nu} = (-4.7 \pm 0.3) \times 10^{-3}$ Hz/s. Uncertainties represent the 1σ confidence intervals derived from the Gaussian fit. Using these parameters, we fold the burst lightcurve with respect to phase. The resulting folded profile is shown in the right panel of Figure 4.

The fractional amplitude of the oscillations can be given by $|A|/\sqrt{2}\bar{R}$, with A the amplitude of the oscillation obtained by fitting the folded profile to a sinusoidal model, \bar{R} the average count rate, determined with the method described in section 2, and a factor $\sqrt{2}$ which allows the fractional amplitude to be given as a rms amplitude. We find a fractional amplitude of $9.6 \pm 1.3\%$ rms in the 4-40 keV energy range. In the 4-10 keV and the 10-20 keV energy ranges, the fractional amplitudes are $2.8 \pm 1.0\%$ and $27.6 \pm 6.1\%$ rms, respectively. In the 20-40 keV range, the flux is too low to allow a reliable computation of the fractional amplitude. We observe an increase in the fractional amplitude with energy, which could indicate a similar origin of oscillations as those observed in some bursts from 4U 1728-34, as described by Mahmoodifar et al. (2019), where oscillations had a strong amplitude in a 6-12 keV energy range but were undetectable in a softer band. Moreover, the mechanism that generates these high-amplitude oscillations in the tail of the burst is unknown, as it requires a luminosity contrast at the neutron star surface. This issue was described by Mahmoodifar & Strohmayer (2016), who proposed cooling models that could explain these phenomena.

4. DISCUSSION

The oscillation frequency that we find with SVOM/ECLAIRs is fully compatible with the signal reported by GECAM (Chen et al. 2022) at 413.63 Hz,

but not the one found with Swift/BAT in a 2006 burst at 414.75 Hz by Strohmayer et al. (2008). To study this discrepancy, we reanalyzed the corresponding archival data using a methodology similar to that described in section 3. The data were retrieved from the Swift Archive² under trigger number 234849 (ObsID 00234849000). We find oscillations $\nu_b = 414.74 \pm 0.02$ Hz within a time window spanning [25 s, 32 s] from the start of the event data, consistent with the value reported in Strohmayer et al. (2008). Uncertainty is given as a 1σ , similarly to Section subsection 3.3. No significant frequency variation is observed, and we place a 95% confidence upper limit on the frequency derivative of $|\dot{\nu}| < 3.4 \times 10^{-2}$ Hz/s. The lower precision of the measurement with respect to the one presented in our work mostly comes from the duration of the respective signals: 7 seconds for the initial discovery and 51 seconds for the burst detected by SVOM/ECLAIRs, as a longer signal allows for a more precise measurement of the frequency drift.

The difference between the frequency measured by Swift/BAT and the frequency measured by SVOM/ECLAIRs at the start of the time window is at least $\Delta\nu = 0.9$ Hz, defined as the distance between their 95% confidence intervals. This corresponds to a spin-down rate of $\dot{\nu} \sim 10^{-9}$ Hz/s, which is too high to be explained by a spin-down of the neutron star alone. For comparison, in accreting millisecond X-ray pulsars, spin-down rates are typically not greater than $\dot{\nu} \sim -10^{-13}$ Hz/s (Patruno & Watts 2020).

Frequency drifts in burst oscillations are most commonly observed as an increase that stabilizes near the neutron star spin frequency (for example, see Figure 2 of Watts 2012). However, spin-down episodes have also been observed in 4U 1636-536 (Strohmayer 1999; Miller 2000), KS 1731-260 (Muno et al. 2000), and 4U 1728-34 (Muno et al. 2002). These spin-down episodes exhibit fractional frequency drifts on the order of $\dot{\nu}/\nu \sim -10^{-3}\text{ s}^{-1}$, which is notably larger than the $\dot{\nu}/\nu \sim -10^{-5}\text{ s}^{-1}$ reported in this work. Moreover, the frequency drift here is apparently constant over the entire duration of the oscillations, which is not the case in spin-down episodes previously reported, where the frequency first increased before decreasing. The differences in both amplitude and temporal regularity may suggest distinct physical origins for the apparent spin-down reported here compared to those in the earlier cases.

If the frequency drift measured in this work originates from the expansion of a shell at radius r , assuming angular momentum conservation, then $\dot{\nu}/\nu = 2\dot{r}/r$.

² <https://www.swift.ac.uk/archive/>

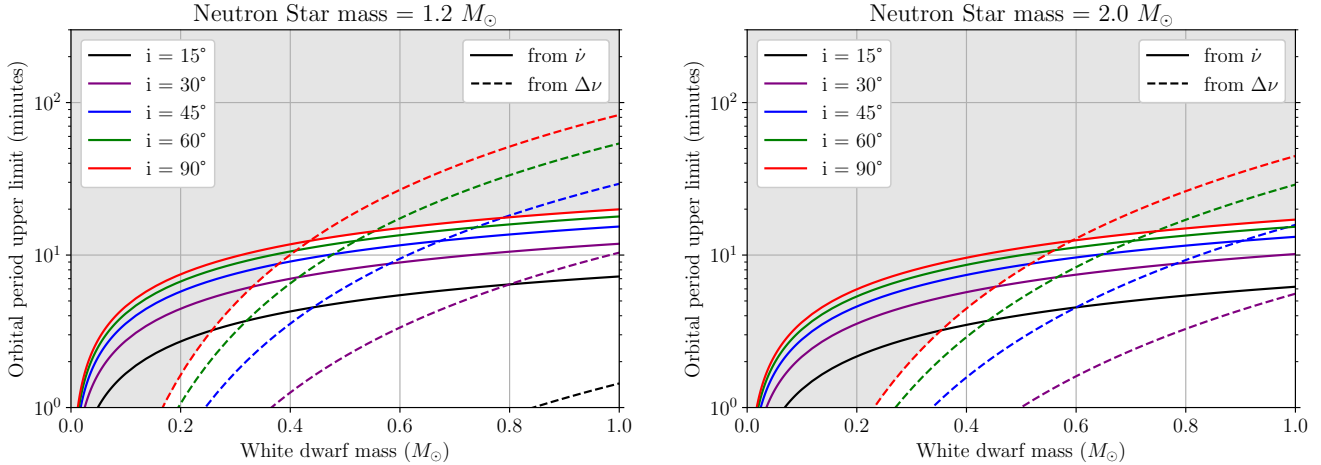


Figure 5. Upper limit of the orbital periods set by the $\Delta\nu$ (dashed lines) and $\dot{\nu}$ (solid lines) as a function of M_{WD} , at different inclinations i , and for $M_{\text{NS}} = 1.2 M_\odot$ (left) and $M_{\text{NS}} = 2.0 M_\odot$ (right). The areas of the parameter space incompatible with the hypothesis that both $\Delta\nu$ and $\dot{\nu}$ originate from orbital motion are represented in gray.

For $r = 6 \text{ km}$, this implies an expansion velocity $\dot{r} \sim 3.4 \text{ cm/s}$, which is compatible with a constant radius as seen on Figure 2. While this scenario is plausible, it fails to explain the steady drift over the entire signal time window; typically, the frequency is expected to increase during the burst tail as the material contracts back onto the neutron star crust (Cumming & Bildsten 2000; Cumming et al. 2002). Therefore, we explore the possibility that the frequency discrepancy between SVOM/ECLAIRs and Swift/BAT $\Delta\nu$ and the frequency drift $\dot{\nu}$ are caused by a Doppler frequency modulation originating from the orbital motion of the binary. Thus, $\Delta\nu$ would be explained by similar frequencies observed at different orbital phases, and $\dot{\nu}$ by the evolution of the radial velocity of the neutron star. Under this hypothesis, the comparable frequencies measured by GECAM and ECLAIRs may indicate that both bursts could have happened on a similar orbital phase.

Assuming that either $\Delta\nu$ or $\dot{\nu}$ is caused by orbital modulation, we aim to constrain the system's orbital parameters (i.e., the orbital period P_{orb} , the masses of the neutron star M_{NS} and white dwarf M_{WD} , and the inclination angle i). This approach is analogous to the analyses by Strohmayer & Markwardt (2002) and Giles et al. (2002), who constrained the masses of the binary components in 4U 1636–53 by inferring the neutron star's orbital velocity from burst oscillations.

If the orbit is circular, then $\Delta\nu$ provides a lower limit on twice the neutron star's maximum radial velocity along its orbit, V_{max} . This, in turn, yields an upper

limit on the ratio P_{orb}/f :

$$2V_{\text{max}} = 2 \left(\frac{2\pi G f}{P_{\text{orb}}} \right)^{1/3} > \frac{c\Delta\nu}{\nu} \Rightarrow \frac{P_{\text{orb}}}{f} < 2\pi G \left(\frac{c\Delta\nu}{2\nu} \right)^{-3}, \quad (1)$$

where f is the system mass function defined as:

$$f = \frac{\sin^3(i) \cdot M_{\text{WD}}^3}{(M_{\text{NS}} + M_{\text{WD}})^2}. \quad (2)$$

Similarly, the maximum radial acceleration \dot{V}_{max} along the orbit must be at least as large as the one inferred from the observed frequency drift $\dot{\nu}$. This leads to an upper limit on the ratio $P_{\text{orb}}/f^{1/4}$:

$$\dot{V}_{\text{max}} = \frac{2\pi}{P_{\text{orb}}} V_{\text{max}} > \frac{c\dot{\nu}}{\nu} \Rightarrow \frac{P_{\text{orb}}}{f^{1/4}} < 2\pi G^{1/4} \left(\frac{c\dot{\nu}}{\nu} \right)^{-3/4}. \quad (3)$$

Figure 5 shows the resulting upper limits on the orbital period derived from Equation 1 and Equation 3, plotted as a function of the white dwarf companion mass for different inclination angles, and assuming two limiting neutron star masses: $1.2 M_\odot$ and $2.0 M_\odot$. We show the entire range of inclination, but it is worth mentioning that Ludlam et al. (2019) finds the inclination of the disk to be between 50° and 62° from a spectral analysis of NuSTAR data. Assuming the observed frequency drift is due to orbital motion, the corresponding orbital period would need to be shorter than approximately 20 minutes with ideal system parameters ($M_{\text{NS}} = 1.2 M_\odot$,

$i = 90^\circ$), or shorter than 15.5 minutes with more realistic parameters $M_{\text{NS}} = 2.0 M_\odot$ (Boutelier et al. 2009) and $i = 62^\circ$ (Ludlam et al. 2019). These values are in tension with previously reported orbital periods for this source, as seen in section 1, but would place the system among the most compact known binaries. On the other hand, it follows from Equation 1 that a physically plausible lower limit on P_{orb} (arbitrarily taken to 1 minute on Figure 5) leads to a lower limit on the mass function f , i.e., a lower limit on M_{WD} for given M_{NS} and inclination. However, these interpretations rely on the assumption that the oscillation frequency is asymptotically stable in the neutron star’s frame and remains consistent across bursts. While the first assumption is supported by the behavior observed in several oscillation detections (see, e.g., Munoz et al. (2002)), the second is more uncertain. For example, Miller (2000) found that frequency variations between bursts of 4U 1636–536 exceeded what would be expected from its orbital motion alone.

5. CONCLUSION

In this Letter, we report the detection by the ECLAIRs coded-mask telescope on board the SVOM satellite of oscillations during a Type-I burst from 4U 0614+091. The oscillations were observed over a 51-second time interval during the burst decay phase, and exhibit a nearly constant frequency drift of $\dot{\nu} = (-4.7 \pm 0.3) \times 10^{-3}$ Hz/s, with an average frequency of $\bar{\nu} = 413.674 \pm 0.002$ Hz. The average frequency is close to, but statistically inconsistent with, the oscillation frequency measured during a previous burst observed by Swift/BAT in 2006. We propose that both the observed frequency offset and the steady drift may

be explained by Doppler modulation due to orbital motion. Under this assumption, the system’s orbital period must be shorter than approximately 20 minutes to account for the observed effects. Further observations are necessary to refine the system’s orbital parameters and assess the viability of the Doppler-modulation scenario. Moreover, an accurate measurement of the short orbital period of this system would make it a validation binary candidate for the Laser Interferometer Space Antenna (LISA, Kupfer et al. 2024). The measurement of a frequency drift with an unprecedented precision demonstrates the remarkable capabilities of SVOM/ECLAIRs for the study of thermonuclear bursts, thanks to its large FoV and good sensitivity in the 5–15 keV range.

¹ This work was supported by CNES, focused on SVOM.
² The Space-based multi-band Variable Objects Monitor (SVOM) is a joint Chinese-French mission led by
³ the Chinese National Space Administration (CNSA),
⁴ the French Space Agency (CNES), and the Chinese
⁵ Academy of Sciences (CAS). We gratefully acknowledge
⁶ the unwavering support of NSSC, IAMCAS, XIOPM,
⁷ NAOC, IHEP, CNES, CEA, CNRS, University of Le-
⁸icester, and MPE. We acknowledge the use of public
⁹ data from the Swift data archive.
¹⁰

Facilities: SVOM (ECLAIRs), Swift (BAT)

Software: numpy (Harris et al. 2020), matplotlib (Hunter 2007), astropy (Astropy Collaboration et al. 2022), stingray (Bachetti et al. 2024b; Huppenkothen et al. 2019; Bachetti et al. 2024a), Xspec (Arnaud 1996)

APPENDIX

A. VALIDATION OF THE TIMING ANALYSIS METHOD ON THE CRAB PULSAR

At the time of the burst from 4U 0614+091, the Crab Nebula was located in ECLAIRs field of view. The Crab pulsar has a frequency of ~ 29.5 Hz, and shows persistent X-ray pulsed emission. This fortuitous observation can be used to validate the analysis procedure described in subsection 3.2, by comparing its timing results to frequency and frequency derivative retrieved from public data from the Jodrell Bank Crab Pulsar Monthly Ephemeris³ (Lyne et al. 1993), issued from radio observations. In a 15-minute observation overlapping the burst, from 2025-01-10T15:53 to 2025-01-10T16:08, pulses from the Crab were detected at a frequency of 29.5529 Hz. The pulsar frequency, computed from radio ephemerides, was at the time 29.5535 Hz, which gives a relative error of $\sim 10^{-5}$. Moreover, no significant frequency drift was observed in this time window, with an upper limit (90% CL) on the frequency derivative of 4×10^{-6} Hz/s, clearly compatible with the actual frequency derivative of the Crab pulsar of $\sim 3 \times 10^{-10}$ Hz/s. Additional checks were performed on a longer (26 ks) pointing of the Crab taken on 2025-02-06. The measured

³ www.jb.man.ac.uk/~pulsar/crab.html

frequency was compatible with radio ephemeris within a relative error of $\sim 10^{-7}$, and no significant frequency drift was measured, with an upper limit of 3×10^{-9} Hz/s. These results indicate no discrepancy between ECLAIRs timing measurements and radio observations. Thus, no systematic timing bias hindering the result presented in this work was found in the telescope data or in the analysis procedure.

REFERENCES

- Arnason, R. M., Papei, H., Barmby, P., Bahramian, A., & Gorski, M. D. 2021, MNRAS, 502, 5455, doi: [10.1093/mnras/stab345](https://doi.org/10.1093/mnras/stab345)
- Arnaud, K. A. 1996, in Astronomical Society of the Pacific Conference Series, Vol. 101, Astronomical Data Analysis Software and Systems V, ed. G. H. Jacoby & J. Barnes, 17
- Astropy Collaboration, Price-Whelan, A. M., Lim, P. L., et al. 2022, ApJ, 935, 167, doi: [10.3847/1538-4357/ac7c74](https://doi.org/10.3847/1538-4357/ac7c74)
- Bachetti, M., Huppenkothen, D., Stevens, A., et al. 2024a, Journal of Open Source Software, 9, 7389, doi: [10.21105/joss.07389](https://doi.org/10.21105/joss.07389)
- Bachetti, M., Huppenkothen, D., Khan, U., et al. 2024b, StingraySoftware/stingray: Stingray v2.2, v2.2, Zenodo, doi: [10.5281/zenodo.13974481](https://doi.org/10.5281/zenodo.13974481)
- Baglio, M. C., Mainetti, D., D'Avanzo, P., et al. 2014, A&A, 572, A99, doi: [10.1051/0004-6361/201424665](https://doi.org/10.1051/0004-6361/201424665)
- Boutelier, M., Barret, D., & Miller, M. C. 2009, MNRAS, 399, 1901, doi: [10.1111/j.1365-2966.2009.15430.x](https://doi.org/10.1111/j.1365-2966.2009.15430.x)
- Buccheri, R., et al. 1983, A&A, 128, 245
- Chen, Y.-P., Li, J., Xiong, S.-L., et al. 2022, ApJ, 935, 10, doi: [10.3847/1538-4357/ac7ff8](https://doi.org/10.3847/1538-4357/ac7ff8)
- Cumming, A., & Bildsten, L. 2000, ApJ, 544, 453–474, doi: [10.1086/317191](https://doi.org/10.1086/317191)
- Cumming, A., Morsink, S. M., Bildsten, L., Friedman, J. L., & Holz, D. E. 2002, ApJ, 564, 343–352, doi: [10.1086/324157](https://doi.org/10.1086/324157)
- Dagoneau, N., & Schanne, S. 2022, A&A, 665, A40, doi: [10.1051/0004-6361/202141891](https://doi.org/10.1051/0004-6361/202141891)
- Dagoneau, N., Schanne, S., Rodriguez, J., Atteia, J.-L., & Cordier, B. 2020, A&A, 645, A18, doi: [10.1051/0004-6361/202038995](https://doi.org/10.1051/0004-6361/202038995)
- Dong, Y., Wu, B., Li, Y., Zhang, Y., & Zhang, S. 2010, Science China Physics, Mechanics and Astronomy, 53, 40, doi: [10.1007/s11433-010-0011-7](https://doi.org/10.1007/s11433-010-0011-7)
- Ford, E., Kaaret, P., Tavani, M., et al. 1997, ApJ, 475, L123, doi: [10.1086/310483](https://doi.org/10.1086/310483)
- Galloway, D. K., in 't Zand, J., Chenevez, J., et al. 2020, The Astrophysical Journal Supplement Series, 249, 32, doi: [10.3847/1538-4365/ab9f2e](https://doi.org/10.3847/1538-4365/ab9f2e)
- Giles, A. B., Hill, K. M., Strohmayer, T. E., & Cummings, N. 2002, ApJ, 568, 279, doi: [10.1086/338890](https://doi.org/10.1086/338890)
- Godet, O., Nasser, G., Atteia, J.-L., et al. 2014, in Space Telescopes and Instrumentation 2014: Ultraviolet to Gamma Ray, ed. T. Takahashi, J.-W. A. den Herder, & M. Bautz, Vol. 9144 (SPIE), 914424, doi: [10.1117/12.2055507](https://doi.org/10.1117/12.2055507)
- Goldwurm, A., & Gros, A. 2022, Coded Mask Instruments for Gamma-Ray Astronomy (Springer Nature Singapore), 1–57, doi: [10.1007/978-981-16-4544-0_44-1](https://doi.org/10.1007/978-981-16-4544-0_44-1)
- Götz, D., Osborne, J., Cordier, B., et al. 2014, in Space Telescopes and Instrumentation 2014: Ultraviolet to Gamma Ray, ed. T. Takahashi, J.-W. A. den Herder, & M. Bautz, Vol. 9144, International Society for Optics and Photonics (SPIE), 914423, doi: [10.1117/12.2054898](https://doi.org/10.1117/12.2054898)
- Harris, C. R., Millman, K. J., van der Walt, S. J., et al. 2020, Nature, 585, 357, doi: [10.1038/s41586-020-2649-2](https://doi.org/10.1038/s41586-020-2649-2)
- Hunter, J. D. 2007, Computing in Science & Engineering, 9, 90, doi: [10.1109/MCSE.2007.55](https://doi.org/10.1109/MCSE.2007.55)
- Huppenkothen, D., Bachetti, M., Stevens, A. L., et al. 2019, ApJ, 881, 39, doi: [10.3847/1538-4357/ab258d](https://doi.org/10.3847/1538-4357/ab258d)
- Kupfer, T., Korol, V., Littenberg, T. B., et al. 2024, LISA Galactic binaries with astrometry from Gaia DR3. <https://arxiv.org/abs/2302.12719>
- Kuulkers, E., in't Zand, J. J. M., Atteia, J. L., et al. 2010, A&A, 514, A65, doi: [10.1051/0004-6361/200913210](https://doi.org/10.1051/0004-6361/200913210)
- Li, Z., Suleimanov, V. F., Poutanen, J., et al. 2018, ApJ, 866, 53, doi: [10.3847/1538-4357/aade8e](https://doi.org/10.3847/1538-4357/aade8e)
- Ludlam, R. M., Miller, J. M., Barret, D., et al. 2019, ApJ, 873, 99, doi: [10.3847/1538-4357/ab0414](https://doi.org/10.3847/1538-4357/ab0414)
- Lyne, A. G., Pritchard, R. S., & Graham Smith, F. 1993, MNRAS, 265, 1003, doi: [10.1093/mnras/265.4.1003](https://doi.org/10.1093/mnras/265.4.1003)
- Madej, O. K., García, J., Jonker, P. G., et al. 2014, MNRAS, 442, 1157–1165, doi: [10.1093/mnras/stu884](https://doi.org/10.1093/mnras/stu884)
- Madej, O. K., Jonker, P. G., Groot, P. J., et al. 2013, MNRAS, 429, 2986, doi: [10.1093/mnras/sts550](https://doi.org/10.1093/mnras/sts550)
- Mahmoodifar, S., & Strohmayer, T. 2016, ApJ, 818, 93, doi: [10.3847/0004-637x/818/1/93](https://doi.org/10.3847/0004-637x/818/1/93)
- Mahmoodifar, S., Strohmayer, T. E., Bult, P., et al. 2019, ApJ, 878, 145, doi: [10.3847/1538-4357/ab20c4](https://doi.org/10.3847/1538-4357/ab20c4)
- Migliari, S., Tomsick, J. A., Miller-Jones, J. C. A., et al. 2010, ApJ, 710, 117, doi: [10.1088/0004-637X/710/1/117](https://doi.org/10.1088/0004-637X/710/1/117)
- Miller, M. C. 2000, ApJ, 531, 458–466, doi: [10.1086/308438](https://doi.org/10.1086/308438)
- Muno, M. P., Chakrabarty, D., Galloway, D. K., & Psaltis, D. 2002, ApJ, 580, 1048, doi: [10.1086/343793](https://doi.org/10.1086/343793)

- Muno, M. P., Fox, D. W., Morgan, E. H., & Bildsten, L. 2000, ApJ, 542, 1016, doi: [10.1086/317031](https://doi.org/10.1086/317031)
- Nelemans, G., Jonker, P. G., Marsh, T. R., & van der Klis, M. 2004, MNRAS, 348, L7–L11, doi: [10.1111/j.1365-2966.2004.07486.x](https://doi.org/10.1111/j.1365-2966.2004.07486.x)
- Patruno, A., & Watts, A. L. 2020, Accreting Millisecond X-ray Pulsars (Springer Berlin Heidelberg), 143–208, doi: [10.1007/978-3-662-62110-3_4](https://doi.org/10.1007/978-3-662-62110-3_4)
- Shahbaz, T., Watson, C. A., Zurita, C., Villaver, E., & Hernandez-Peralta, H. 2008, PASP, 120, 848, doi: [10.1086/590505](https://doi.org/10.1086/590505)
- Strohmayer, T. E. 1999, ApJ, 523, L51, doi: [10.1086/312258](https://doi.org/10.1086/312258)
- Strohmayer, T. E., & Markwardt, C. B. 2002, ApJ, 577, 337–345, doi: [10.1086/342152](https://doi.org/10.1086/342152)
- Strohmayer, T. E., Markwardt, C. B., & Kuulkers, E. 2008, ApJL, 672, L37, doi: [10.1086/526546](https://doi.org/10.1086/526546)
- Strohmayer, T. E., Zhang, W., Swank, J. H., et al. 1996, ApJL, 469, L9, doi: [10.1086/310261](https://doi.org/10.1086/310261)
- van Doesburgh, M., van der Klis, M., & Morsink, S. M. 2018, MNRAS, 479, 426, doi: [10.1093/mnras/sty1404](https://doi.org/10.1093/mnras/sty1404)
- Watts, A. L. 2012, ARA&A, 50, 609, doi: [10.1146/annurev-astro-040312-132617](https://doi.org/10.1146/annurev-astro-040312-132617)
- Wei, J., Cordier, B., Antier, S., et al. 2016, The Deep and Transient Universe in the SVOM Era: New Challenges and Opportunities - Scientific prospects of the SVOM mission. <https://arxiv.org/abs/1610.06892>
- Wu, C., Qiu, Y. L., & Cai, H. B. 2012, in IAU Symposium, Vol. 279, Death of Massive Stars: Supernovae and Gamma-Ray Bursts, ed. P. Roming, N. Kawai, & E. Pian, 421–422, doi: [10.1017/S1743921312013646](https://doi.org/10.1017/S1743921312013646)